























**Table 7.** Bias and RSME (in Parentheses) of Regional FPAR and LAI Predictions by PFT With the Prior Parameter Set and the Parameters Constrained by the 256 Region Experiment<sup>a</sup>

PFT	FPAR		LAI	
	Prior	256	Prior	256
bar all	0.30 (0.31)	<b>-0.01 (0.02)</b>	1.62 (1.63)	<b>0.02 (0.04)</b>
enf tem	<b>0.02 (0.10)</b>	<b>-0.02 (0.03)</b>	0.93 (1.11)	<b>-0.17 (0.33)</b>
enf bor	-0.12 (0.22)	<b>0.00 (0.05)</b>	0.32 (1.14)	<b>0.03 (0.16)</b>
dnf bor	-0.06 (0.21)	<b>0.00 (0.08)</b>	0.56 (1.32)	<b>0.03 (0.23)</b>
ebf tro	0.06 (0.06)	<b>0.01 (0.02)</b>	<b>0.01 (0.23)</b>	<b>0.19 (0.27)</b>
ebf tem	<b>0.04 (0.12)</b>	<b>0.00 (0.02)</b>	0.62 (0.93)	<b>0.25 (0.41)</b>
dbf tro	0.16 (0.17)	<b>0.00 (0.01)</b>	1.36 (1.39)	<b>0.08 (0.15)</b>
dbf tem	0.07 (0.12)	<b>-0.03 (0.04)</b>	1.07 (1.26)	<b>-0.09 (0.38)</b>
dbf bor	<b>-0.00 (0.21)</b>	<b>-0.00 (0.07)</b>	0.68 (1.39)	<b>0.19 (0.42)</b>
ebs all	<b>0.01 (0.16)</b>	<b>-0.04 (0.07)</b>	0.79 (1.07)	<b>-0.10 (0.27)</b>
dbs tem	0.33 (0.33)	<b>0.04 (0.04)</b>	2.14 (2.17)	<b>0.25 (0.26)</b>
dbs bor	<b>-0.04 (0.18)</b>	<b>0.01 (0.07)</b>	0.61 (1.18)	<b>0.04 (0.15)</b>
c3g arc	<b>0.02 (0.13)</b>	<b>-0.00 (0.03)</b>	0.76 (1.16)	<b>0.03 (0.09)</b>
c3g nar	0.27 (0.28)	<b>0.02 (0.03)</b>	1.95 (1.99)	<b>0.11 (0.13)</b>
c4g all	0.26 (0.27)	<b>0.01 (0.02)</b>	2.09 (2.10)	<b>0.10 (0.12)</b>

<sup>a</sup>The accuracy of bold values is better than 5% of the full FPAR or LAI range (1.0 and 8.0, respectively).

given in Table 7 clearly demonstrate that both magnitude (bias) and phase (rmse) significantly gain in realism. Bold values document that for all PFTs the FPAR and LAI biases fall below 5% of the FPAR and LAI range, while most rmse values reach this threshold in the 256 region experiment.

### 3.4. Local Prediction

[44] Any scientific application that is applied to global scales should be reevaluated at the local scale if possible in order to gain a better process-based understanding and reveal missing model components [see, e.g., *Stöckli et al.*, 2008a; *Oleson et al.*, 2008]. The phenology model using the global parameter set has therefore been tested at the same four FLUXNET tower sites as in our local-scale data assimilation study [*Stöckli et al.*, 2008b]. The aim of this section is to evaluate to what degree the model using the above estimated global parameter set is still able to represent local-scale phenology at specific sites.

#### 3.4.1. Morgan Monroe State Forest

[45] The Morgan Monroe State Forest site (USA) is a temperate deciduous forest interleaved by grassland and crops. The site-level simulation and the 4 region experiment simulate a realistic seasonal cycle (Figure 6a). The 4 region experiment should always be closer to the site-level experiment than for instance the 256 region experiment since the former uses parameters that are constrained over exactly the four regions covering the four sites, where the latter uses parameters that minimize the prediction error for a global area. A two-stage green-up successively appears in the 16, 64 and 256 region experiments. This two-stage green-up is likely due to a unrealistic green-up timing of nonnatural PFTs present in this grid cell. The PFT parameters for maize (14% of the area) and soy (12% of the area) are constrained with information from globally distributed croplands by the 16, 64 and 256 region experiments, but their values do not seem to be valid at this particular site or for this particular year. The employed static PFT map would firstly not be suitable in areas where crop rotation is practiced, and secondly a crop

phenology model might be required to realistically simulate the phenological stages of different crops in a global prediction. Senescence is realistic in the 4, 16, 64 and 256 region experiments but is delayed in the site-level experiment. The 64 and 256 region experiments further reveal a underestimation of summer LAI magnitude. It might be related to the negative bias of the temperate deciduous broadleaf forest LAI prediction found in the regional analysis above (Table 7).

#### 3.4.2. BOREAS Old Black Spruce

[46] The high prediction skill at the boreal forest site BOREAS Old Black Spruce (Canada) appears to be independent of whether a site-level or global parameter set is used (Figure 6b). This result firstly demonstrates that the regions where boreal evergreen needleleaf forest occur are spatially more homogeneous than for instance the patchy landscapes encountered in temperate climate zones. The PFT distribution at BOREAS for instance consists of around 50% evergreen needleleaf trees, 20% deciduous shrubs and 20% Arctic grasslands. Secondly, phenological timing for this PFT is controlled by a well defined set of environmental triggers (defined by the climate control parameters in Table 3) that are valid from local to global scales. This result is underlined by the high prediction performance of the boreal evergreen needleleaf forest PFT found in the regional analysis above.

#### 3.4.3. Santarem KM83

[47] The prior parameter set at the tropical evergreen broadleaf site Santarem KM83 (Brazil) creates a unrealistic light-limited leaf loss of around  $2 \text{ m}^2 \text{ m}^{-2}$  at the end of the wet season (April–June) while both quality screened observations and all posterior parameter sets show a constant LAI throughout the year. Figure 6c demonstrates that the employed observation quality control is working well and that cloud affected (wet season) and aerosol contaminated (dry season) observations at the site are properly screened and do not affect the data assimilation process.

#### 3.4.4. Tonzi Ranch

[48] Although the Tonzi site (USA) has the same mean monthly precipitation and mean temperature as Morgan Monroe State Forest (the two red boxes that coincide in the center of Figure 1b), it is a mediterranean savanna-type ecosystem with a rather dry late summer and a wet winter season. Figure 6d shows that the magnitude but also the timing of the drought response between May and September (see also Figures 3 and 4 in the work of *Stöckli et al.* [2008b]) are simulated very realistically by the site-level and the 4 region experiments compared to the prior experiment. The timing is still accurate in the 16, 64 and 256 region experiments, but the peak LAI during April and May is severely underestimated in the 16, 64 and 256 region experiments. The result demonstrates that global parameter sets can become inaccurate at the local scale for ecosystems with a complex canopy. The site-level experiment yields July/August LAI values that are comparable to ground measurements [*Ryu et al.*, 2010b]. However, our simplified canopy radiative transfer neglects the contribution of vegetation structural aspects like leaf clumping while ground measurements often neglect the contribution of the understory LAI that is also measured by the satellite. Currently the comparison of satellite- and ground-observed phenology is best achieved through the analysis of phenological timing [*Studer et al.*, 2007; *Stöckli et al.*, 2008b; *Liang et al.*, 2011]. Newly developed near-surface remote sensing methods are promis-

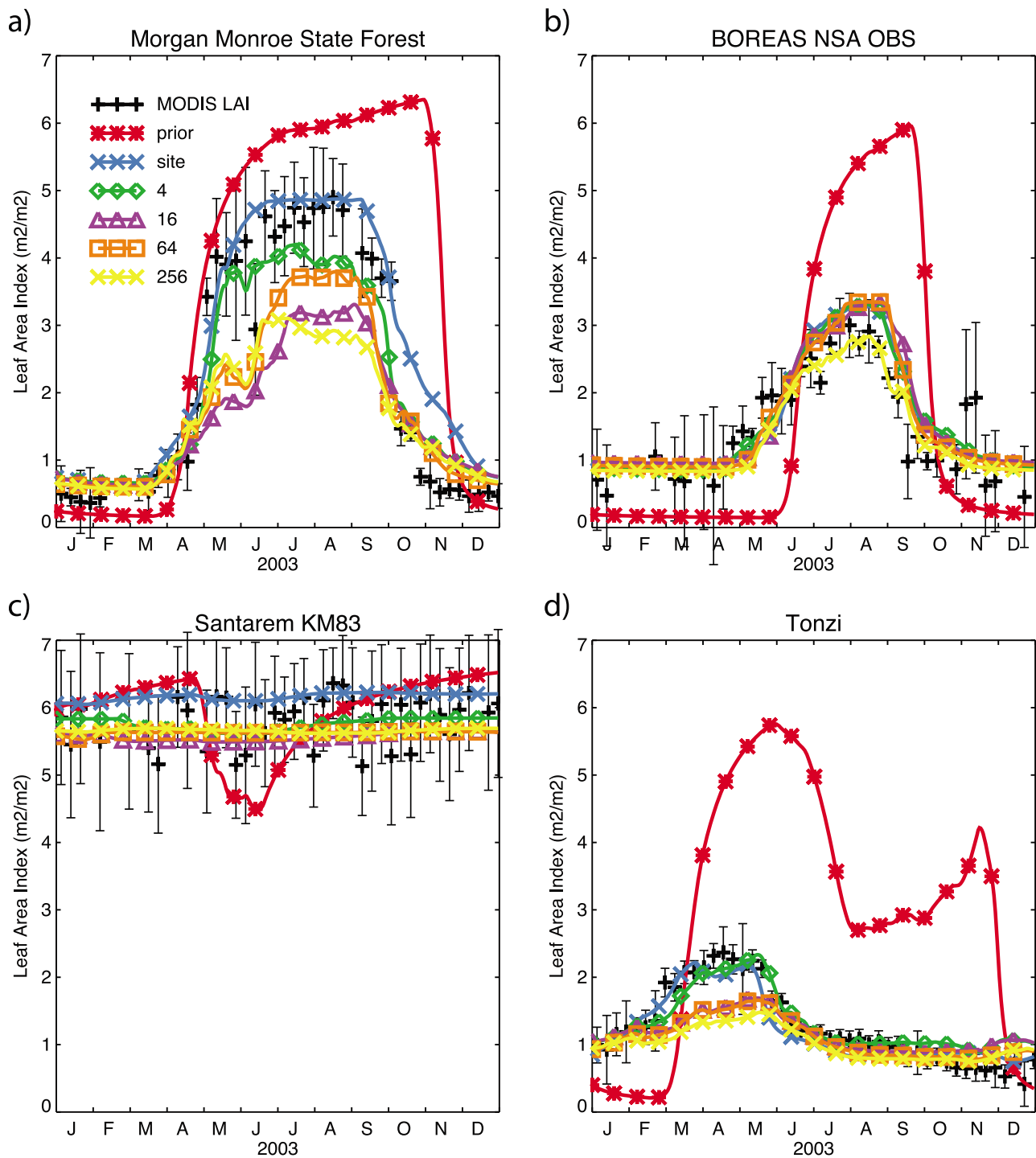


**Figure 6.** Predicted versus observed site-level ( $0.5^\circ \times 0.5^\circ$ ) LAI using the site-level, the prior parameter set and the parameter sets constrained by 4, 16, 64 and 256 regions during 2003.

ing to also compare phenological magnitude [Ahrends *et al.*, 2008; Richardson *et al.*, 2009; Ryu *et al.*, 2010a].

## 4. Discussion

### 4.1. Data Assimilation

[49] By running the data assimilation over less than 1% of the global land surface the global FPAR and LAI prediction error could be reduced to below 20% of its initial value. The

key for this success is most likely the wide climatic and biogeographic range spanned by the chosen subset of assimilation regions (Figure 1). The 4 region experiment already includes a tropical, a temperate, a boreal and a mediterranean climatic environment to constrain a set of parameters that then show substantial skill in a global prediction (Figure 3). Figure 4 suggests that little improvement can be expected when extending the assimilation area beyond the 0.4% of global land area covered by the 256 region experi-

ment. Research on the optimal location of assimilation regions might further reduce the computational resources needed for a global data assimilation of vegetation phenology.

[50] The parameter uncertainties seem to converge much faster than the prediction errors. While the EnKF allows in theory a perfect estimation of the combined posterior model and parameter error by analysis of both the prior model uncertainty and the observation uncertainty, there are many assumptions to be made for the practical implementation of the EnKF in a prediction system. Each of the following assumptions could be the cause for the observed parameter overconfidence:

[51] 1. The ensemble size  $N$  for the EnKF should be as large as possible since the sampling error decreases by  $1/\sqrt{N}$ . 1000 ensemble members are likely too low since around 10000 states and 510 parameters are estimated for each region. With the available computational resources for this project there is little that can be done regarding ensemble size.

[52] 2. If the measurement size exceeds the ensemble size, rank problems can occur because the measurement error covariance needs to be compressed into the ensemble space. We however make use of the inversion presented by Evensen [2004] that uses a measurement operator covering the full rank of measurements to avoid the problem of rank loss reported in the literature [Kepert, 2004].

[53] 3. If the measurement uncertainty is poorly chosen in a bayesian method, the posterior model uncertainty will likely be wrong. The measurement uncertainty is derived from MODIS quality flags that are themselves based on semiempirical detection algorithms for clouds, shadows, aerosols and reflect an incomplete set of retrieval errors [Justice et al., 2002]. Further, arbitrary scaling factors are used to transfer the quality flags into a quantitative set of observation uncertainties. The superobservations derived in equation (29) neglect any spatially correlated measurement errors that are likely to happen with cloud contamination or snow cover.

[54] 4. The EnKF solver is chosen to avoid local minima since the full nonlinear prediction model is integrated without the need to create first order derivatives as needed for instance in the Extended Kalman Filter or in variational data assimilation techniques like 3D or 4D VAR. A yearly analysis guarantees that parameters do not satisfy individual observations but are consistent with the entire seasonal cycle of the leaf state.

[55] 5. By estimating a set of 15 parameters for a total of 34 PFTs several solutions in the parameter space might produce a similar prediction. However, even though equifinality might generate wrong parameters it should to the best of our knowledge not lead to parameter overconfidence.

## 4.2. Phenology Model

[56] We chose a rather empirical phenology model with a large set of climate control parameters, structural vegetation parameters and time averaging parameters.

[57] It was demonstrated how both climate control and structural vegetation parameters can be thoroughly constrained by the 10 years of MODIS data while time averaging parameters are left with a substantial posterior uncertainty. There is nevertheless evidence that the time averaging needed

for temperature and light are likely shorter than 21 days and the averaging time for moisture is higher than 21 days. This result contrasts most temperature-based phenology models that work with growing degree days since they often integrate temperature history over several months [Chuine, 2000]. The long averaging time for moisture further demonstrate that tall trees in temperate climate zones can sustain greenness for prolonged periods of droughts. For short natural vegetation like grasslands and deciduous shrubs the moisture averaging times result well below 21 days, most likely related to their short rooting depths and higher susceptibility to drought.

[58] The tropical evergreen broadleaf forest PFT requires the longest moisture averaging times. Our model yields a seasonally largely constant FPAR and LAI for this PFT. Tropical trees are known to be resistant to the yearly recurring dry periods [Lee et al., 2005]. Recent studies however demonstrate that tropical plant physiology and phenology is very complex and both can sensitive to extreme drought periods [Saleska et al., 2007; Myneni et al., 2007; Phillips et al., 2009; Zhao and Running, 2010]. These studies are based on satellite-based EVI, modeled GPP or on field measurements of biochemical fluxes and carbon stocks and not on satellite-based FPAR or LAI. Further, drought-induced changes in tropical phenology may not be detectable with spectroradiometers like MODIS but only with hyperspectral radiometers like Hyperion [Asner et al., 2004]. These open questions should motivate follow-up research in both modeling and observation of tropical phenology.

[59] Our model entirely depends on a multiplicative set of linearized and time integrated temperature, light and moisture controls. The model therefore excludes several known biophysical and abiotic controls such as chilling requirements, insect pests, harvest, irrigation, nutrient limitations, tree aging, biodiversity effects or frost events. The high prediction skill on the seasonal and interannual timescale spanning local to global spatial scales demonstrates that the main drivers of phenological variability have been included in the model. However, the short observation period of 10 years by definition excludes most climatological extreme events required to exploit the full range seasonal to decadal phenological variability. Especially the climate control parameters of subtropical and tropical drought-deciduous PFTs might benefit from a longer observation period.

[60] Plant physiological research suggests that bud burst of temperate deciduous species is driven by photoperiod (but not necessarily the light intensity  $R_g$  as used in this study). Photoperiod can serve as trigger for temperature sensitivity [Körner, 2006]. Our results demonstrate that the best empirical prediction of temperate deciduous broadleaf forest phenology is simulated by a combined temperature-light forcing. Figure 4a of Stöckli et al. [2008b] visualizes that a light trigger (green curve, crosses) precedes the temperature trigger (red curve, stars). However, it is currently debated whether light, temperature or both control bud burst. These relationships also vary by species [Körner and Basler, 2010] and cannot be generalized [Cleland et al., 2007].

## 4.3. Plant Functional Type Data

[61] Plant functional types [Bonan et al., 2002] are chosen instead of the often used biomes or land cover classes [Hansen et al., 2000] because they are better in line with the

separation needed for phenological predictions. The single savanna biome at for instance the Tonzi Ranch is composed of a evergreen broadleaf tree PFT (with maximum LAI in late summer) and of a drought-deciduous c3 grass PFT (with maximum LAI in early spring). Both PFTs display a very different phenological cycle and there is no single parameter set that would enable a realistic simulation of the single savanna biome. The regional analysis however suggests that several PFT classes like the temperate deciduous broadleaf forest PFT, the evergreen broadleaf shrub PFT or the temperate deciduous broadleaf shrub PFT might still be too heterogeneous in terms of phenological behavior and could be separated into sub-PFT classes. Phenological predictions would surely benefit from consistent global PFT maps based on new remote sensing technologies as for instance presented by *Ustin and Gamon* [2010].

[62] The focus of this study is the estimation of phenology parameters for natural vegetation. However, crop PFTs were also included in the data assimilation. Satellite pixels contain a mixed signal from both natural and managed vegetation that needs to be decomposed in order to estimate parameters for the natural vegetation PFTs. Figure 3 demonstrates that the FPAR and LAI of regions with heavy crop cover are well predicted without the explicit use of a crop phenology model. This shows that even managed vegetation phenology is dominantly weather and climate driven. However, for climate model applications a dedicated crop phenology model should be used since especially the carbon uptake of crops differs from natural vegetation [*Gervois et al.*, 2004; *Lokupitiya et al.*, 2009].

#### 4.4. Satellite Data

[63] The MODIS FPAR and LAI data are derived from MODIS surface reflectances by inversion of a canopy radiative transfer model [*Myneni et al.*, 1999, 2002]. They are more accurate in low biomass areas and generally exaggerate LAI for broadleaf and needleleaf forests [*Wang et al.*, 2004; *Cohen et al.*, 2006]. The LAI retrieval from visible and near-infrared surface reflectances is underdetermined for intermediate and high LAI values which can yield errors in the order of 50% [*Garrigues et al.*, 2008]. The FPAR and LAI data set presented in this study will inherit such errors. We further use a very simplified representation of the canopy light interception that only fits 4 canopy structural parameters per PFT ( $FPAR_{min}$ ,  $FPAR_{max}$ ,  $FPAR_{sat}$  and  $LAI_{max}$ ). Compared to the MODIS retrieval algorithm it does not include the effects of foliage and canopy clumping, nongreen canopy elements, soil background reflectance, shading or vertical canopy structure [*Myneni et al.*, 1999; *Shabanov et al.*, 2003]. These differences can introduce inconsistencies between the assimilated and predicted FPAR and LAI values. They might be responsible for some of the scaling issues found at Morgan Monroe and Tonzi Ranch.

[64] The restrictive quality screening of MODIS observations employed in this study eliminates the majority of cloud, aerosol, snow and cloud shadow contamination that usually complicates the generation of climate quality biophysical satellite parameters in tropical or high latitude [*Los et al.*, 2000; *Poulter and Cramer*, 2009]. On the global average 40–50% of all valid observations pass quality screening (Table 6). In tropical areas only 5–10% (not shown) pass

the quality screening. Neglecting quality screening can for instance lead to misleading conclusions on the drought response of tropical trees [*Saleska et al.*, 2007] as shown by *Samanta et al.* [2010].

[65] Remote sensing data assimilation in combination with a predictive model has the capability to complement the classical data-only gap filling procedures such as maximum value compositing or fourier time series fitting employed in most current satellite-based land surface data sets [*Los et al.*, 2000; *Jonsson and Eklundh*, 2002; *Stöckli and Vidale*, 2004; *Tucker et al.*, 2005; *Fang et al.*, 2008].

#### 4.5. Weather Forcing Data

[66] The model parameter set and therefore the phenological prediction will be sensitive to the choice of weather forcing data since predicted states are empirically and not mechanistically linked to the meteorological predictors. Potential biases in the ECMWF ERA Interim data might therefore have created unrealistic posterior parameter sets during the data assimilation. We have perturbed the weather forcing data with uncertainties as given in section 2, but the perturbation does not correct for biases in the weather forcing data. Also, a new estimation of model parameters might be required if a new weather forcing data with a different spatial scale or with a different climatology is used or if the phenology model is applied in coupled mode as part of a climate model.

### 5. Conclusions and Outlook

[67] Our study demonstrates how remote sensing data assimilation can be used to reduce uncertainties in a global phenology model. The assimilation of MODIS data covering less than 1% of the global land surface successfully reduced the global FPAR and LAI prediction errors to 20.6% and 14.8% of their respective prior errors. A too high variance reduction in the posterior parameter set could be mitigated by use of a more quantitative observation uncertainty estimation. Novel data assimilation methods such as the Maximum Likelihood Ensemble Filter MLEF [*Zupanski*, 2005] employing Hessian preconditioning and a gradient search method might yield more realistic globally applicable parameter sets.

[68] Our study suggests that PFTs are a suitable means to disaggregate mixed satellite pixels on global scale and they allow to create a PFT-specific parameterization of a globally applicable phenology model. The boreal evergreen needleleaf forest PFT and the tropical evergreen broadleaf forest PFT perform realistically over a large range of spatial scales. However, local-scale predictions using a global parameter set can become unreliable in both magnitude and timing as for instance demonstrated for the mixed natural-agricultural temperate landscape (Morgan Monroe) and the savanna landscape (Tonzi Ranch). The phenological data assimilation experiment could now be repeated with a variety of globally applicable phenology models and PFT data sets. In order to increase the compatibility between assimilated and predicted vegetation states the MODIS canopy radiative transfer model could be employed in the prediction of FPAR and LAI. A more complex treatment of leaf and canopy clumping, leaf orientation, shadowing or nongreen canopy elements would further broaden the applicability of our methods and data sets.

As a first step global maps of foliage clumping [Chen *et al.*, 2005; Pisek *et al.*, 2010] could enhance our simplified LAI calculation with geometric information on canopy structure.

[69] Our study is a first step to mitigate some deficiencies of current phenological models. As already shown by Stöckli *et al.* [2008b] the parameterized phenology model can be useful to disentangle the influence of meteorological drivers on the observed phenological variability. It could be a contribution to the currently ongoing discussion on how temperature and light (or photoperiod) govern the timing of phenological spring events [Körner and Basler, 2010]. The 50 year long global phenological reanalysis data set (1960–2009) should be suitable for climate analysis studies. It might for instance contain evidence on whether the light trigger is the hard limit for the currently observed (temperature-related) negative trends for phenological spring events [Cleland *et al.*, 2007; Rutishauser *et al.*, 2007].

[70] Future research should combine process-based knowledge from hydrology, plant physiology and canopy radiative transfer modeling with the highly empirical world of plant phenology. This is needed to better understand and simulate the response of the terrestrial water and carbon cycle to climate variability and change and to quantify the resulting impacts on the other earth system components [Penuelas *et al.*, 2009]. We would therefore like to motivate earth system modelers to experiment with data assimilation and to bring forward a new generation of phenology and land surface models. In order to facilitate this, the presented data set, all program codes, parameters, documentation and simple hands-on experiments are publicly available at <http://phenoanalysis.sourceforge.net>.

## Appendix A: Plant Functional Type Data Generation

[71] The following modifications are made to the PFT processing by Lawrence and Chase [2007] and Bonan *et al.* [2002]:

[72] 1. The single crop class is decomposed into 19 individual crop classes according to Leff *et al.* [2004].

[73] 2. This yields 35 PFT classes in total: 15 natural types, 19 crop classes and water.

[74] 3. The processing is performed at 30" spatial resolution instead of 0.05°.

[75] 4. The monthly temperature climatology [Wilmott and Matsuura, 2007] is downscaled to 30" by use of a lapse rate of 0.5 K 100 m<sup>-1</sup> applied to the above described topography data set.

[76] 5. MOD15A2 LAI is quality screened as described above in order to evaluate the c4 grass fraction. Following Still *et al.* [2003] the c4 grass fraction is the sum of LAI for those months that satisfy the c4 growth criteria (temperature >22°C and precipitation >25 mm) over the sum of LAI for all months. Since they have used NDVI instead of LAI, we apply the square-root to the LAI-derived c4 grass fraction in order to account for the almost exponential relationship between NDVI and LAI.

[77] 6. The processing merges 7 sometimes inconsistent data sets into a single continuous plant functional type cover data set. The inconsistencies (e.g. MOD44B indicates 25% tree cover but the AVHRR VCF shows 0% tree cover) are

overcome by inverse distance filling where the MODIS data set served as the reference data set.

## Appendix B: Technical Set Up

[78] The data assimilation framework is parallelized by using Version 1.2 of the MPI standard [Message P Forum, 1994] with a one- or two-dimensional process topology (multiple regions and one region per process, or single region distributed along longitude and latitude range). Model state prediction, I/O, observation QA screening, gridding of superobservations, **HA** and **D** matrices are calculated on separate processes by assigning one region per process and one process by logical CPU unit. The prior parameters are perturbed once and distributed to all processes in order to end up with a global analysis parameter set. Model states and weather forcing are perturbed by process. One process is reserved for the global analysis, where all regional **HA** and **D** are collected at the end of each simulation year and the global analysis is performed. The global analysis matrix (X5 of Evensen [2003]) is finally redistributed to all processes, where the computationally intensive final ensemble update of states and parameters is performed.

[79] The bottlenecks for this framework are its heavy memory usage, the size of the observational data and the global EnKF analysis. The parallelization of the EnKF solver would be an important next step in order to increase data assimilation performance. The state matrix has 7 dimensions (ens × lon × lat × PFT × HGT × state × days), the parameter matrix has 3 dimensions (ens × PFT × parameter), the forcing data has 5 dimensions (ens × lon × lat × HGT × forcing), which exceeds per-process memory availability on today's supercomputers. In order to increase memory efficiency, a subset of HGT and PFT classes for states is integrated in each region, where only HGT and PFT classes are selected that cover more than 2.5% of the area in each region. Water areas (PFT number 35) are screened and not used during the analysis. Furthermore the upper bound of superobservations to be used in the global analysis was set to 50000. The analysis then is within around 1 GB per process (with a maximum of 4–8 GB per node on, e.g., NCCS Discover with 8 CPUs per node and 16–32 GB per node on, e.g., NCAR Bluefire with 32 CPUs per node).

[80] **Acknowledgments.** The NASA Energy and Water Cycle Study (NEWS) grant NNG06CG42G, NASA grant NNX11AB87G and MeteoSwiss provided funding for this study. The MODIS Science Team and the MODIS Science Data Support Team provided the MOD15A2, MOD44B and MOD12Q1 data. The NASA Science Mission Directorate (SMD) is acknowledged for granting the SMD-08-0810 and SMD-09-1256 requests with 250,000 and 460,000 CPU hours, respectively, on the NASA Center for Computational Sciences (NCCS) High-End Computing (HEC) Discover system. The National Center for Atmospheric Research (NCAR) Terrestrial Sciences Section (TSS) is acknowledged for providing computational resources on the Bluefire system for testing purposes. The Swiss Center for Scientific Computing (CSCS) is acknowledged for providing computational resources on the Rigi system for testing purposes.

## References

- Ahrends, H. E., R. Bruegger, R. Stöckli, J. Schenk, P. Michna, F. Jeanneret, H. Wanner, and W. Eugster (2008), Quantitative phenological observations of a mixed beech forest in northern Switzerland with digital photography, *J. Geophys. Res.*, *113*, G04004, doi:10.1029/2007JG000650.
- Arora, V. K., and G. J. Boer (2005), A parameterization of leaf phenology for the terrestrial ecosystem component of climate models, *Global Change Biol.*, *11*(1), 39–59, doi:10.1111/j.1365-2486.2004.00890.x.

- Asner, G., D. Nepstad, G. Cardinot, and D. Ray (2004), Drought stress and carbon uptake in an Amazon forest measured with spaceborne imaging spectroscopy, *Proc. Natl. Acad. Sci. U. S. A.*, *101*(16), 6039–6044, doi:10.1073/pnas.0400168101.
- Berrisford, P., D. Dee, K. Fielding, M. Fuentes, P. Kallberg, S. Kobayashi, and S. Uppala (2009), The ERA-Interim archive version 1.0, *ERA Rep. Ser. 1*, Eur. Cent. for Medium-Range Weather Forecasts, Reading, U. K.
- Betts, A. K., and P. Viterbo (2005), Land-surface, boundary layer, and cloud-field coupling over the southwestern Amazon in ERA-40, *J. Geophys. Res.*, *110*, D14108, doi:10.1029/2004JD005702.
- Betts, A. K., R. L. Desjardins, and D. Worth (2007), Impact of agriculture, forest and cloud feedback on the surface energy budget in boreas, *Agric. For. Meteorol.*, *142*(2–4), 156–169.
- Bonan, G. B. (2002), *Ecological Climatology*, Cambridge Univ. Press, Cambridge, U. K.
- Bonan, G. B., S. Levis, L. Kergoat, and K. W. Oleson (2002), Landscapes as patches of plant functional types: An integrating concept for climate and ecosystem models, *Global Biogeochem. Cycles*, *16*(2), 1021, doi:10.1029/2000GB001360.
- Chen, J., C. Menges, and S. Leblanc (2005), Global mapping of foliage clumping index using multi-angular satellite data, *Remote Sens. Environ.*, *97*(4), 447–457, doi:10.1016/j.rse.2005.05.003.
- Chuine, I. (2000), A unified model for budburst of trees, *J. Theor. Biol.*, *207*, 337–347.
- Cleland, E. E., I. Chuine, A. Menzel, H. A. Mooney, and M. D. Schwartz (2007), Shifting plant phenology in response to global change, *Trends Ecol. Evol.*, *22*(7), 357–365, doi:10.1016/j.tree.2007.04.003.
- Cohen, W. B., et al. (2006), Modis land cover and LAI collection 4 product quality across nine sites in the western hemisphere, *IEEE Trans. Geosci. Remote Sens.*, *44*(7), 1843–1857.
- Cox, P. M. (2001), Description of the TRIFFID dynamic global vegetation model, *Tech. Rep. 24*, Hadley Cent., Bracknell, U. K.
- Defries, R. S., M. C. Hansen, J. R. G. Townshend, A. C. Janetos, and T. R. Loveland (2000), A new global 1-km dataset of percentage tree cover derived from remote sensing, *Global Change Biol.*, *6*(2), 247–254.
- Demarty, J., F. Chevallier, A. D. Friend, N. Viovy, S. Piao, and P. Ciais (2007), Assimilation of global MODIS leaf area index retrievals within a terrestrial biosphere model, *Geophys. Res. Lett.*, *34*, L15402, doi:10.1029/2007GL030014.
- Dickinson, R. E., Y. Tian, Q. Liu, and L. Zhou (2008), Dynamics of leaf area for climate and weather models, *J. Geophys. Res.*, *113*, D16115, doi:10.1029/2007JD008934.
- Evensen, G. (1994), Sequential data assimilation with a nonlinear quasi-gestrophic model using Monte-Carlo methods to forecast error statistics, *J. Geophys. Res.*, *99*(C5), 10,143–10,162.
- Evensen, G. (2003), The ensemble kalman filter: Theoretical formulation and practical implementation, *Ocean Dyn.*, *53*, 343–367.
- Evensen, G. (2004), Sampling strategies and square root analysis schemes for the EnKF, *Ocean Dyn.*, *54*(6), 539–560.
- Evensen, G. (2009), The ensemble kalman filter for combined state and parameter estimation, *IEEE Control Syst. Mag.*, *29*, 83–104.
- Fang, H. L., S. L. Liang, J. R. Townshend, and R. E. Dickinson (2008), Spatially and temporally continuous LAI data sets based on an integrated filtering method: Examples from North America, *Remote Sens. Environ.*, *112*, 75–93.
- Farquhar, G. D., S. V. Caemmerer, and J. A. Berry (1980), A biochemical model of photosynthetic CO<sub>2</sub> assimilation in leaves of C-3 species, *Planta*, *149*, 78–90.
- Fisher, J. I., J. F. Mustard, and M. A. Vadeboncoeur (2006), Green leaf phenology at Landsat resolution: Scaling from the field to the satellite, *Remote Sens. Environ.*, *100*(2), 265–279.
- Foley, J. A., I. C. Prentice, N. Ramankutty, S. Levis, D. Pollard, S. Sitch, and A. Haxeltine (1996), An integrated biosphere model of land surface processes, terrestrial carbon balance, and vegetation dynamics, *Global Biogeochem. Cycles*, *10*(4), 603–628.
- Friedl, M. A., et al. (2002), Global land cover mapping from MODIS: Algorithms and early results, *Remote Sens. Environ.*, *83*, 287–302.
- Garrigues, S., et al. (2008), Validation and intercomparison of global leaf area index products derived from remote sensing data, *J. Geophys. Res.*, *113*, G02028, doi:10.1029/2007JG000635.
- Gervois, S., N. de Noblet-Ducoudre, N. Viovy, and P. Ciais (2004), Including croplands in a global biosphere model: Methodology and evaluation at specific sites, *Earth Interactions*, *8*(16), 1–25.
- Hansen, M., R. Defries, J. Townshend, M. Carroll, C. Dimiceli, and R. Sohlberg (2003), Global percent tree cover at a spatial resolution of 500 meters: First results of the modis vegetation continuous fields algorithm, *Earth Interactions*, *7*(10), 1–15.
- Hansen, M. C., R. Defries, J. R. G. Townshend, and R. Sohlberg (2000), Global land cover classification at 1km spatial resolution using a classification tree approach, *Int. J. Remote Sens.*, *21*(6/7), 1331–1364.
- Heck, P., D. Luthi, and C. Schär (1999), The influence of vegetation on the summertime evolution of European soil moisture, *Phys. Chem. Earth B*, *24*, 609–614.
- Jarvis, P. G. (1976), The interpretation of the variations in leaf water potential and stomatal conductance found in canopies in the field, *Philos. Trans. R. Soc. London, Ser. B*, *273*, 593–610.
- Jolly, W. M., R. Nemani, and S. W. Running (2005), A generalized, bioclimatic index to predict foliar phenology in response to climate, *Global Change Biol.*, *11*, 619–632.
- Jonsson, P., and L. Eklundh (2002), Seasonality extraction by function fitting to time-series of satellite sensor data, *IEEE Trans. Geosci. Remote Sens.*, *40*, 1824–1832.
- Justice, C. O., J. R. G. Townshend, E. F. Vermote, E. Masuoka, R. E. Wolfe, N. Saleous, D. P. Roy, and J. T. Morisette (2002), An overview of MODIS land data processing and product status, *Remote Sens. Environ.*, *83*, 3–15.
- Keeling, C. D., J. F. S. Chin, and T. P. Whorf (1996), Increased activity of northern vegetation inferred from atmospheric CO<sub>2</sub> measurements, *Nature*, *382*, 146–149.
- Keper, J. D. (2004), On ensemble representation of the observation—Error covariance in the ensemble Kalman filter, *Ocean Dyn.*, *6*, 561–569.
- Kim, Y., and G. L. Wang (2005), Modeling seasonal vegetation variation and its validation against Moderate Resolution Imaging Spectroradiometer (MODIS) observations over North America, *J. Geophys. Res.*, *110*, D04106, doi:10.1029/2004JD005436.
- Knorr, W., T. Kaminski, M. Scholze, N. Gobron, B. Pinty, R. Giering, and P. P. Mathieu (2010), Carbon cycle data assimilation with a generic phenology model, *J. Geophys. Res.*, *115*, G04017, doi:10.1029/2009JG001119.
- Körner, C. (2003), Slow in, rapid out—Carbon flux studies and Kyoto targets, *Science*, *300*, 1242–1243.
- Körner, C. (2006), Significance of temperature in plant life, in *Plant Growth and Climate Change*, pp. 48–69, Blackwell, Oxford, U. K.
- Körner, C., and D. Basler (2010), Phenology under global warming, *Science*, *327*, 1461–1462.
- Kramer, K., I. Leinonen, and D. Loustau (2000), The importance of phenology for the evaluation of impact of climate change on growth of boreal, temperate and mediterranean forests ecosystems: An overview, *Int. J. Biometeorol.*, *44*, 67–75.
- Kucharik, C. J., C. C. Barford, M. E. Maayar, S. C. Wofsy, R. K. Monson, and D. D. Baldocchi (2006), A multiyear evaluation of a Dynamic Global Vegetation Model at three AmeriFlux forest sites: Vegetation structure, phenology, soil temperature, and CO<sub>2</sub> and H<sub>2</sub>O vapor exchange, *Ecol. Modell.*, *196*(1–2), 1–31.
- Larcher, W. (2003), *Physiological Plant Ecology: Ecophysiology and Stress Physiology of Functional Groups*, 4th ed., Springer, Heidelberg, Germany.
- Law, B., et al. (2002), Environmental controls over carbon dioxide and water vapor exchange of terrestrial vegetation, *Agric. For. Meteorol.*, *113*, 97–120.
- Lawrence, P. J., and T. N. Chase (2007), Representing a new MODIS consistent land surface in the Community Land Model (CLM 3.0), *J. Geophys. Res.*, *112*, G01023, doi:10.1029/2006JG000168.
- Lee, J.-E., R. S. Oliveira, T. E. Dawson, and I. Fung (2005), Root functioning modifies seasonal climate, *Proc. Natl. Acad. Sci. U. S. A.*, *102*(49), 17,576–17,581.
- Leff, B., N. Ramankutty, and J. A. Foley (2004), Geographic distribution of major crops across the world, *Global Biogeochem. Cycles*, *18*, GB1009, doi:10.1029/2003GB002108.
- Levis, S., and G. B. Bonan (2004), Simulating springtime temperature patterns in the community atmosphere model coupled to the community land model using prognostic leaf area, *J. Clim.*, *17*(23), 4531–4540.
- Li, H., E. Kalnay, and T. Miyoshi (2009), Simultaneous estimation of covariance inflation and observation errors within an ensemble kalman filter, *Q. J. R. Meteorol. Soc.*, *135*, 523–533.
- Liang, L., M. D. Schwartz, and S. Fei (2011), Validating satellite phenology through intensive ground observation and landscape scaling in a mixed seasonal forest, *Remote Sens. Environ.*, *115*, 143–157.
- Lokupitiya, E., et al. (2009), Incorporation of crop phenology in simple biosphere model (sibcrop) to improve land-atmosphere carbon exchanges from croplands, *Biogeosciences*, *6*, 969–986.
- Los, S. O., et al. (2000), A global 9-yr biophysical land surface dataset from NOAA AVHRR data, *J. Hydrometeorol.*, *1*, 183–199.
- Lu, L., R. A. P. Sr, G. E. Liston, W. J. Parton, D. Ojima, and M. Hartman (2001), Implementation of a two-way interactive atmospheric and ecological model and its application to the central United States, *J. Clim.*, *14*, 900–919.
- Mahadevan, P., et al. (2008), A satellite-based biosphere parameterization for net ecosystem CO<sub>2</sub> exchange: Vegetation Photosynthesis and Respi-

- ration Model (VPRM), *Global Biogeochem. Cycles*, 22, GB2005, doi:10.1029/2006GB002735.
- Menzel, A., et al. (2006), European phenological response to climate change matches the warming pattern, *Global Change Biol.*, 12, 1969–1976, doi:10.1111/j.1365-2486.2006.01193.x.
- Message P Forum (1994), MPI: A message-passing interface standard, *Tech. Rep. UT-CS-94-230*, Univ. of Tenn., Knoxville.
- Monsi, M., and T. Saeki (2005), On the factor light in plant communities and its importance for matter production, *Ann. Bot.*, 95, 549–567.
- Moradkhani, H., S. Sorooshian, H. V. Gupta, and P. R. Houser (2005), Dual stateparameter estimation of hydrological models using ensemble Kalman filter, *Adv. Water Resour.*, 28, 135–147.
- Myneni, R. B., Y. Knyazikhin, Y. Zhang, Y. Tian, Y. Wang, and A. Lotsch (1999), Modis leaf area index (LAI) and fraction of photosynthetically active radiation absorbed by vegetation (FPAR) product (mod15), in *Algorithm Theoretical Basis Document Version 4.0*, Sch. of For., Univ. of Mont., Missoula.
- Myneni, R. B., et al. (2002), Global products of vegetation leaf area and fraction absorbed PAR from year one of MODIS data, *Remote Sens. Environ.*, 83, 214–231.
- Myneni, R. B., et al. (2007), Large seasonal swings in leaf area of Amazon rainforests, *Proc. Natl. Acad. Sci.*, doi:10.1073/pnas.0611338104.
- Oleson, K. W., et al. (2008), Improvements to the Community Land Model and their impact on the hydrological cycle, *J. Geophys. Res.*, 113, G01021, doi:10.1029/2007JG000563.
- Penuelas, J., T. Rutishauser, and I. Filella (2009), Phenology feedbacks on climate change, *Science*, 324(5929), 887–888, doi:10.1126/science.1173004.
- Phillips, O. L., et al. (2009), Drought sensitivity of the Amazon rainforest, *Science*, 323(5919), 1344–1347, doi:10.1126/science.1164033.
- Piao, S., P. Friedlingstein, P. Ciais, N. Viovy, and J. Demarty (2007), Growing season extension and its impact on terrestrial carbon cycle in the Northern Hemisphere over the past 2 decades, *Global Biogeochem. Cycles*, 21, GB3018, doi:10.1029/2006GB002888.
- Pisek, J., J. M. Chen, R. Lacaze, O. Sonnentag, and K. Alikas (2010), Expanding global mapping of the foliage clumping index with multi-angular polder three measurements: Evaluation and topographic compensation, *ISPRS J. Photogramm. Remote Sens.*, 65(4), 341–346, doi:10.1016/j.isprsjprs.2010.03.002.
- Poulter, B., and W. Cramer (2009), Satellite remote sensing of tropical forest canopies and their seasonal dynamics, *Int. J. Remote Sens.*, 30(24), 6575–6590, doi:10.1080/01431160903242005.
- Randerson, J. T., et al. (2009), Systematic assessment of terrestrial biogeochemistry in coupled climate-carbon models, *Global Change Biol.*, 15(10), 2462–2484, doi:10.1111/j.1365-2486.2009.01912.x.
- Rayner, P. J. (2010), The current state of carbon-cycle data assimilation, *Curr. Opinion Environ. Sustainability*, 2(4), 289–296, doi:10.1016/j.cosust.2010.05.005.
- Richardson, A. D., B. H. Braswell, D. Y. Hollinger, J. P. Jenkins, and S. V. Ollinger (2009), Near-surface remote sensing of spatial and temporal variation in canopy phenology, *Ecol. Appl.*, 19(6), 1417–1428.
- Rüdiger, C., C. Albergel, J.-F. Mahfouf, J.-C. Calvet, and J. P. Walker (2010), Evaluation of the observation operator Jacobian for leaf area index data assimilation with an extended Kalman filter, *J. Geophys. Res.*, 115, D09111, doi:10.1029/2009JD012912.
- Rutishauser, T., J. Luterbacher, F. Jeanneret, C. Pfister, and H. Wanner (2007), A phenology-based reconstruction of interannual changes in past spring seasons, *J. Geophys. Res.*, 112, G04016, doi:10.1029/2006JG000382.
- Ryu, Y., D. D. Baldocchi, J. Verfaillie, S. Ma, M. Falk, I. Ruiz-Mercado, T. Hehn, and O. Sonnentag (2010a), Testing the performance of a novel spectral reflectance sensor, built with light emitting diodes (LEDs), to monitor ecosystem metabolism, structure and function, *Agric. For. Meteorol.*, 150(12), 1597–1606, doi:10.1016/j.agrformet.2010.08.009.
- Ryu, Y., O. Sonnentag, T. Nilson, R. Vargas, H. Kobayashi, R. Wenk, and D. D. Baldocchi (2010b), How to quantify tree leaf area index in an open savanna ecosystem: A multi-instrument and multi-model approach, *Agric. For. Meteorol.*, 150(1), 63–76, doi:10.1016/j.agrformet.2009.08.007.
- Saleska, S. R., K. Didan, A. R. Huete, and H. R. da Rocha (2007), Amazon forests green-up during 2005 drought, *Science*, 318(5850), 612, doi:10.1126/science.1146663.
- Samanta, A., S. Ganguly, H. Hashimoto, S. Devadiga, E. Vermote, Y. Knyazikhin, R. R. Nemani, and R. B. Myneni (2010), Amazon forests did not green-up during the 2005 drought, *Geophys. Res. Lett.*, 37, L05401, doi:10.1029/2009GL042154.
- Schaefer, K., A. S. Denning, and O. Leonard (2005), The winter Arctic Oscillation, the timing of spring, and carbon fluxes in the Northern Hemisphere, *Global Biogeochem. Cycles*, 19, GB3017, doi:10.1029/2004GB002336.
- Scheffinger, H., A. Menzel, E. Koch, C. Peter, and R. Ahas (2002), Atmospheric mechanisms governing the spatial and temporal variability of phenological phases in central Europe, *Int. J. Climatol.*, 22, 1739–1755.
- Schimel, D. S., B. H. Braswell, and W. J. Parton (1997), Equilibration of the terrestrial water, nitrogen, and carbon cycles, *Proc. Natl. Acad. Sci. U. S. A.*, 94(16), 8280–8283.
- Sellers, P. J., S. O. Los, C. J. Tucker, C. O. Justice, D. A. Dazlich, G. J. Collatz, and D. A. Randall (1996a), A revised land surface parameterization (SiB2) for atmospheric GCMs. 2. The generation of global fields of terrestrial biophysical parameters from satellite data, *J. Clim.*, 9, 706–737.
- Sellers, P. J., D. A. Randall, G. J. Collatz, J. A. Berry, C. B. Field, D. A. Dazlich, C. Zhang, G. D. Collelo, and L. Bounoua (1996b), A revised land surface parameterization (SiB2) for atmospheric GCMs. 1. Model formulation, *J. Clim.*, 9, 676–705.
- Sellers, P. J., et al. (1997), Modeling the exchanges of energy, water, and carbon between continents and the atmosphere, *Science*, 275(5299), 502–509.
- Shabanov, N. V., Y. Wang, W. Buermann, J. Dong, S. Hoffman, G. R. Smith, Y. Tian, Y. Knyazikhin, and R. B. Myneni (2003), Effect of foliage spatial heterogeneity in the MODIS LAI and FPAR algorithm over broadleaf forests, *Remote Sens. Environ.*, 85, 410–423.
- Stich, S., et al. (2003), Evaluation of ecosystem dynamics, plant geography and terrestrial carbon cycling in the LPJ dynamic global vegetation model, *Global Change Biol.*, 9(2), 161–185.
- Still, C. J., J. A. Berry, G. J. Collatz, and R. S. DeFries (2003), Global distribution of C<sub>3</sub> and C<sub>4</sub> vegetation: Carbon cycle implications, *Global Biogeochem. Cycles*, 17(1), 1006, doi:10.1029/2001GB001807.
- Stöckli, R., and P. Vidale (2004), European plant phenology and climate as seen in a 20-year AVHRR land-surface parameter dataset, *Int. J. Remote Sens.*, 25(17), 3303–3330, doi:10.1080/01431160310001618149.
- Stöckli, R., D. M. Lawrence, G. Y. Niu, K. W. Oleson, P. E. Thornton, Z. L. Yang, G. B. Bonan, A. S. Denning, and S. W. Running (2008a), Use of FLUXNET in the Community Land Model development, *J. Geophys. Res.*, 113, G01025, doi:10.1029/2007JG000562.
- Stöckli, R., T. Rutishauser, D. Dragoni, J. O’Keefe, P. E. Thornton, M. Jolly, L. Lu, and A. S. Denning (2008b), Remote sensing data assimilation for a prognostic phenology model, *J. Geophys. Res.*, 113, G04021, doi:10.1029/2008JG000781.
- Studer, S., R. Stöckli, C. Appenzeller, and P. L. Vidale (2007), A comparative study of satellite and ground-based phenology, *Int. J. Biometeorol.*, 51(5), 405–414, doi:10.1007/s00484-006-0080-5.
- Taylor, K. E. (2001), Summarizing multiple aspects of model performance in a single diagram, *J. Geophys. Res.*, 106(D7), 7183–7192.
- Thornton, P. E., et al. (2002), Modeling and measuring the effects of disturbance history and climate on carbon and water budgets in evergreen needleleaf forests, *Agric. For. Meteorol.*, 113(1–4), 185–222.
- Thornton, P. E., J.-F. Lamarque, N. A. Rosenbloom, and N. Mahowald (2007), Influence of carbon-nitrogen cycle coupling on land model response to CO<sub>2</sub> fertilization and climate variability, *Global Biogeochem. Cycles*, 21, GB4018, doi:10.1029/2006GB002868.
- Tsvetinskaya, E. A., L. O. Mearns, and W. E. Easterling (2001), Investigating the effect of seasonal plant growth and development in three-dimensional atmospheric simulations. part I: Simulation of surface fluxes over the growing season, *J. Clim.*, 14(5), 692–709.
- Tucker, C. J., J. E. Pinzon, M. E. Brown, D. A. Slayback, E. W. Pak, R. Mahoney, E. F. Vermote, and N. E. Saleous (2005), An extended AVHRR 8-km NDVI dataset compatible with MODIS and SPOT vegetation NDVI data, *Int. J. Remote Sens.*, 26(20), 4485–4498.
- Uppala, S. M., et al. (2005), The ERA-40 re-analysis, *Q. J. R. Meteorol. Soc.*, 131(612), 2961–3012.
- U.S. Geological Survey (1996), GTOPO30, digital media, Sioux Falls, S. D.
- Ustin, S. L., and J. A. Gamon (2010), Remote sensing of plant functional types, *New Phytol.*, 186, 795–816.
- van Vliet, A. J. H., et al. (2003), The European Phenology Network, *Int. J. Biometeorol.*, 47(4), 202–212.
- Wang, Y. J., et al. (2004), Evaluation of the MODIS LAI algorithm at a coniferous forest site in Finland, *Remote Sens. Environ.*, 91, 114–127.
- Wilmott, C. J., and K. Matsuura (2007), Global air temperature and precipitation: Regrided monthly and annual climatologies (v 2.01 for precip and v 2.02 for temperature), Univ. of Delaware, Newark. (Available at [http://climate.geog.udel.edu/climate/html\\_pages/download.html](http://climate.geog.udel.edu/climate/html_pages/download.html).)

Zhao, M., and S. W. Running (2010), Drought-induced reduction in global terrestrial net primary production from 2000 through 2009, *Science*, 329(5994), 940–943, doi:10.1126/science.1192666.

Zupanski, M. (2005), Maximum likelihood ensemble filter: Theoretical aspects, *Mon. Weather Rev.*, 133(6), 1710–1726.

M. A. Liniger and R. Stöckli, Climate Services, Climate Analysis, Federal Office of Meteorology and Climatology MeteoSwiss, Krähbühlstrasse 58, CH-8044 Zürich, Switzerland. (reto.stoeckli@meteoswiss.ch)

T. Rutishauser, Institute of Geography, University of Bern, CH-3012 Bern, Switzerland.

---

I. Baker and A. S. Denning, Department of Atmospheric Science, Colorado State University, Fort Collins, CO 80523, USA.